Iranian Radiation Protection Society

Original Scientific Paper

Journal of Radiation Safety and Measurement

Vol. 15, No. 1, Spring 2026, Pages 1-14

Received: 20 July 2025, Accepted: 29 October 2025

RBS Magnetic Hyperthermia Treatment of Lung Cancer Using Fe_3O_4 Nanoparticles with Silver Shielding for Cardiac Protection

Kazhal Moetamedi[1], Mohammad Hossein Tavakoli*[,1], Safoora Nikzad[2] and Zahra Keshtpour Amlashi[3]

[1]Department of Physics, Faculty of Sciences, Bu-Ali Sina University, Hamedan, Iran.
[2]Isfahan University of Medical Sciences, Hezar Jerib Avenue, Isfahan, Iran.
[3]Cancer Research Center, Institute of Cancer, Avicenna Health Research Institute, Hamadan University of Medical Sciences, Hamadan, Iran.
Email: mht@basu.ac.ir

Abstract

Magnetic hyperthermia using Fe_3O_4 nanoparticles offers a targeted and minimally invasive strategy for lung cancer treatment. In this study, a two dimensional computational model was developed in COMSOL Multiphysics 6.1 to simulate heat generation by uniformly distributed Fe_3O_4 nanoparticles under a 300 kHz, 150 A alternating magnetic field. The model incorporated anatomically realistic domains representing the lung, tumor, and heart tissues, along with a silver shielding layer designed to attenuate magnetic flux and protect the heart from excessive heating. Electromagnetic and thermal behavior were modeled using Maxwell's equations and a porous-media form of Pennes' bioheat equation, accounting for blood perfusion, respiratory airflow, and metabolic heat generation. Simulation results demonstrated that the tumor core reaches therapeutic hyperthermia levels (43-46 °C), while the silver shield effectively maintains cardiac temperatures below 39 °C. Temperature gradients at the tumor margins, caused by convective cooling, highlight the importance of optimizing nanoparticle concentration and field intensity. This model provides a physiologically realistic and computationally validated framework that enhances the safety and efficacy of magnetic hyperthermia, supporting its potential translation into clinical applications.

Keywords: Magnetic hyperthermia, Fe_3O_4 nanoparticles, Lung cancer treatment, Silver shielding, Cardiac protection, Electromagnetic simulation, Heat transfer, Targeted therapy.

1. INTRODUCTION

Lung cancer remains one of the leading causes of cancer-related mortality worldwide, accounting for a significant proportion of cancer diagnoses and deaths annually [1]. Conventional treatments, including surgery, chemotherapy, and radiotherapy, often have limited efficacy and substantial side effects due to damage to surrounding healthy tissues [2]. Therefore, there is an urgent need for targeted, minimally invasive therapeutic strategies that can effectively eradicate tumor cells while preserving healthy organs.

Magnetic hyperthermia therapy (MHT) has gained considerable attention as a promising modality for cancer treatment. This technique involves the administration of magnetic nanoparticles (MNPs), typically iron oxide-based such as Fe_3O_4, which generate localized heat upon exposure to an alternating magnetic field (AMF) [3,4]. The induced heat raises the temperature of tumor tissues to approximately 42–45°C, causing selective tumor cell death without harming adjacent normal tissues [4].

Despite the advantages of MHT, a critical challenge remains in protecting vital organs located near the tumor site, such as the heart in the case of lung cancer. Exposure to magnetic fields and subsequent heating may lead to unintended thermal damage, posing significant risks to cardiac function [5]. To address this issue, recent studies have explored the use of shielding materials to attenuate magnetic field penetration into sensitive regions [6].

In this study, we propose the use of a silver shielding layer surrounding the heart to mitigate magnetic field exposure and prevent overheating during magnetic hyperthermia treatment of lung cancer. Silver is selected due to its excellent electrical conductivity and biocompatibility, enabling efficient attenuation of electromagnetic fields while maintaining patient safety [7]. A two-dimensional computational model is developed to simulate the thermal and electromagnetic interactions within lung, tumor, heart, and shield regions under a 300 kHz AMF. The efficacy of the silver shield in protecting cardiac tissue without compromising tumor hyperthermia is investigated.

Silver was chosen due to its superior electrical conductivity (6.30×10^7 S/m) compared with gold (4.10×10^7 S/m) and copper (5.96×10^7 S/m), allowing more effective attenuation of electromagnetic fields. Moreover, silver exhibits high biocompatibility, intrinsic antimicrobial activity, and lower density, making it particularly suitable for biomedical shielding applications where both electromagnetic efficiency and tissue safety are essential.

This work aims to provide insights into optimizing magnetic hyperthermia protocols with enhanced organ protection, advancing the clinical applicability of nanoparticle-mediated cancer therapies.

2. MATERIALS AND METHODS

2.1 PROBLEM DEFINITION

A two-dimensional (2D) computational model was developed to investigate magnetic nanoparticle-mediated hyperthermia (MNH) as a localized treatment for lung cancer using Fe_3O_4 (magnetite) nanoparticles. The model captures a cross-sectional anatomical representation of lung tissue containing a tumor mass positioned adjacent to the heart, allowing for simultaneous analysis of thermal effects on both cancerous and

critical healthy tissues. The lung region was modeled as a porous biological medium with realistic thermal and physiological properties, incorporating blood perfusion and metabolic heat generation. The tumor was idealized as a circular domain with a diameter of 1 cm, consistent with clinically relevant early-stage lung tumors, and was assumed to contain a uniform distribution of Fe_3O_4 nanoparticles.

To prevent unintended heating of cardiac tissue during hyperthermia treatment, a silver shielding layer was introduced around the heart region. Silver was selected due to its high electrical conductivity and biocompatibility, serving as an effective electromagnetic shield to attenuate magnetic field penetration while minimizing thermal conduction to surrounding tissues.

The model incorporated coupled electromagnetic and thermal physics, solving Maxwell's equations for the alternating magnetic field at 300kHz frequency and an applied current of 150A, parameters chosen to reflect clinically safe and effective hyperthermia protocols. Heat generation from the nanoparticles was modeled considering Néel and Brownian relaxation mechanisms, converting magnetic energy into localized thermal energy within the tumor site.

Thermal transport was governed by the Penne's bioheat equation, accounting for conduction, blood perfusion, and metabolic heat sources in the heterogeneous tissue environment. The computational domain was discretized using the finite element method (FEM) with a fine triangular mesh to ensure numerical accuracy and convergence. The primary objective was to elevate tumor temperature within the therapeutic range of 42-46°C, sufficient to induce apoptosis and inhibit tumor growth, while maintaining heart tissue temperature within physiological limits to avoid thermal damage. The model enabled evaluation of the shielding effectiveness of silver in reducing magnetic flux density and thermal load on cardiac tissue during hyperthermia treatment. This simulation provides insight into optimizing magnetic hyperthermia parameters and shielding strategies, contributing to safer and more effective lung cancer therapies. Figure 1 shows a view of the problem geometry and its meshing.

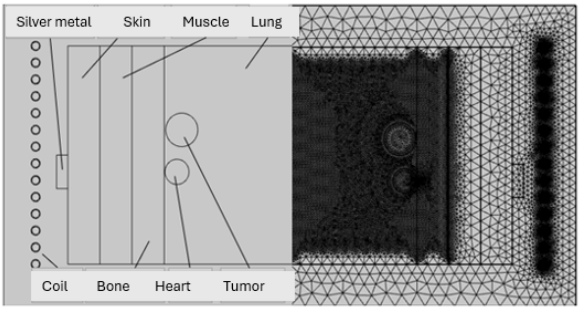

Figure (1). View of the studied system (left) and the meshing of the problem (right)

2.2 MATHEMATICAL MODEL

The thermal response of lung tissue during magnetic nanoparticle-mediated hyperthermia (MNH) was modeled by solving a set of coupled partial differential equations that govern heat transfer and nanoparticle interactions within heterogeneous biological tissues. The model considered multiple layers including porous lung parenchyma, bone, muscle, and skin, each assigned specific thermal and physiological properties such as thermal conductivity, density, specific heat capacity, and blood perfusion rate.

To accurately capture the influence of respiration on heat distribution, dynamic airflow was incorporated within the porous lung domain. This approach simulates the

convective heat transport caused by breathing cycles, which affects temperature gradients and the spatial behavior of nanoparticles during exposure to the alternating magnetic field (AMF). The interaction between airflow and thermal conduction provides a more physiologically realistic environment for evaluating treatment outcomes.

The heating effect generated by Fe_3O_4 nanoparticles results from magnetic energy dissipation through Néel and Brownian relaxation mechanisms triggered by the applied AMF. This localized heat source was integrated into the bioheat transfer framework to simulate the temperature elevation within the tumor region.

By combining detailed anatomical heterogeneity, physiological airflow effects, and nanoparticle-induced heating, the model offers a comprehensive platform to predict temperature distributions during MNH treatment. This allows for optimization of critical parameters such as nanoparticle concentration, AMF frequency and intensity, and treatment duration, with the aim of maximizing tumor ablation while minimizing damage to surrounding healthy tissues.

The heat generated in the tumor tissue by the magnetic nanoparticles is described by the following equation [30-35].

$$p = \mu_0 \pi x_0 f H^2 \frac{2\pi f \tau}{1+(2\pi f \tau)^2} \quad (1)$$

In this equation, μ_0 is the permeability of free space, x_0 is the magnetic susceptibility, H and f represent the intensity and frequency of the alternating magnetic field, and τ is the effective relaxation time, which is obtained from the following relation:

$$\tau = \frac{\tau_B \tau_N}{\tau_B + \tau_N} \quad (2)$$

In this equation, τ_B and τ_N represent the Brownian and Néel relaxation times, respectively, which are obtained from the following relations:

$$\Gamma = \frac{KV_M}{K_B T} \quad (3)$$

$$\tau_N = \frac{\sqrt{\pi}}{2} \tau_0 \frac{\exp(\Gamma)}{\sqrt{\Gamma}} \quad (4)$$

$$\tau_B = \frac{3\eta V_H}{K_B T} \quad (5)$$

In this equation, η is the viscosity of the fluid, V_H is the hydrodynamic volume of the nanoparticles, K_a is the Boltzmann constant, τ_0 is the mean relaxation time in response to thermal equilibrium, and T is the absolute temperature.

The heat transfer in biological tissues is commonly described using Pennes' bioheat equation. This equation considers the effect of blood perfusion on temperature distribution and has been widely used in thermal modeling of tumors. However, in this study, a porous media approach is adopted to better represent lung tissue characteristics, where heat exchange between blood and tissue is modeled using local thermal equilibrium assumptions. This equation has been applied in modeling heat transfer in laryngeal tissue [29,34]:

$$\rho_1 c_1 \frac{\partial T}{\partial t} = \nabla.(k\nabla T) - \rho_b c_b w_b (T - T_b) + Q_{met} + p \quad \text{tumor} \quad (6)$$

$$\rho_1 c_1 \frac{\partial T}{\partial t} = \nabla.(k\nabla T) - \rho_b c_b w_b (T - T_b) + Q_{met} \quad \text{tissue} \quad (7)$$

Where ρ is the density, c is the specific heat, k is the tissue thermal conductivity, T is the tissue temperature, w_b is the blood perfusion, Q_{met} is the metabolic heat generation rate of the tissue, and p is the heat generated by the nanoparticles.

The introduction of a porous medium model accounts for the unique structure of lung tissue, where air-filled alveoli and capillary networks significantly influence heat transfer. This adjustment leads to a more

accurate prediction of temperature gradients within the tumor and surrounding lung tissue.

The Pennes biological heat transfer equation was modified to obtain a heat transfer model based on porous media. The local thermal equilibrium assumption is also used, and the temperature field of the lung tissue can be obtained by calculation, considering that the blood and the lung tissue have the same temperature [36-40].

The equation is shown as follows:

$$(\rho c)_{eff}\frac{\partial T}{\partial t} + (\rho c)_b\left(u\frac{\partial T}{\partial r} + w\frac{\partial T}{\partial z}\right) = k_{eff}\left(\frac{\partial^2 T}{\partial r^2} + \frac{\partial^2 T}{\partial z^2}\right) + Q_{met} + Q_{ext} \quad (8)$$

$$(\rho c)_{eff} = (1-\varphi)(\rho c)_s + \varphi(\rho c)_b \quad (9)$$

$$k_{eff} = (1-\varphi)k_s + \varphi k_b \quad (10)$$

where φ is the porosity of porous media, subscripts eff, s, and b represent the effective value, solid phase (i.e., lung tissue), and liquid phase (i.e., blood) [41,42].

Moreover, the extent of tumor tissue destruction is computed using the degradation integral $\Omega(t)$, based on the first-order Arrhenius equation. In this equation, the relationship between tissue death, temperature, and treatment time is given by the following expression.

$$\Omega(t) = \int_0^t A \cdot e^{Ea/RT,} dt \quad (11)$$

The calculation of thermal degradation in the laryngeal region is based on temperature, exposure time to heat, and other parameters, where *t* is the erosion time, *A* is the frequency factor, Ea is the activation energy for the irreversible degradation reaction, and R is the universal gas constant [43-48]. it is other parameters are shown in Table 1.

The boundary conditions considered for the Pennes bioheat equation are as follows:

1. At the upper and lower boundaries, the heat flux is zero ($\frac{\partial n}{\partial T} = 0$).
2. The body surface temperature is considered to be 37°C.

For the purposes of computational feasibility and model tractability, two simplifying assumptions were adopted: (1) a uniform distribution of Fe_3O_4 nanoparticles within the tumor domain, and (2) local thermal equilibrium (LTE) between blood and surrounding tissue. While these assumptions may not fully reflect in vivo heterogeneity in nanoparticle uptake or temperature gradients at capillary scales, they are widely used in preliminary thermal modeling of biological tissues. These simplifications enable focused analysis of key electromagnetic and thermal effects and provide a reliable approximation framework for early-stage simulation studies. Future work may involve incorporating heterogeneous nanoparticle distributions and two-phase thermal modeling to more closely reflect biological conditions.

Parameter	ρ[kg/m³]	c[J/kg.K]	k [W/m.K]
Normal	1043	3639	0.515
Tumor	1060	3650	0.535
Blood	1050	4180	0.510
Fe_3O_4	5180	4000	40

Table (1). Values of parameters used [49].

2.3 CALCULATION CONDITIONS

The simulation results highlight the critical influence of the lung's porous microstructure on heat transfer dynamics during magnetic nanoparticle-mediated hyperthermia. The lung tissue, characterized by air-filled alveoli interspersed with vascularized regions, creates a complex thermal environment where significant temperature gradients arise between the tumor and surrounding healthy tissues. This heterogeneous architecture plays a pivotal role in modulating the spatial distribution of heat, emphasizing the necessity of

incorporating accurate tissue morphology and properties into computational models. Fe_3O_4 nanoparticles exhibited strong magnetic responsiveness, effectively generating localized thermal energy within the tumor when subjected to an alternating magnetic field (AMF). However, due to the porous nature of lung tissue, some degree of heat dissipation into adjacent structures was observed, which may reduce thermal efficiency if not properly accounted for. These findings underscore the importance of precise modeling of both nanoparticle distribution and tissue heterogeneity to accurately predict thermal outcomes. Furthermore, while Fe_3O_4 nanoparticles possess a high specific absorption rate (SAR), optimizing their concentration alongside AMF parameters such as frequency and field intensity is essential. This optimization ensures adequate tumor heating to induce therapeutic hyperthermia while preventing excessive thermal exposure to nearby sensitive organs, particularly the heart. Collectively, these insights advocate for patient-specific computational modeling to tailor hyperthermia treatment plans. By thoroughly understanding the interactions between nanoparticle heating, tissue structural complexity, and heat diffusion mechanisms, clinicians and researchers can enhance the safety and efficacy of magnetic nanoparticle-mediated hyperthermia as a treatment modality for lung cancer.

3. RESULTS

This study systematically investigates the thermal effects of the porous lung environment on magnetic nanoparticle-mediated hyperthermia (MNH) for lung cancer treatment using a comprehensive computational model. The simulation conditions include a very low concentration of Fe_3O_4 nanoparticles (0.00004 mg/mL), an alternating magnetic field frequency of 300 kHz, and dynamic consideration of respiratory mechanics and airflow within the lung. The results demonstrate that even at this low nanoparticle concentration, sufficient localized heating can be achieved, raising tumor temperatures to the therapeutic range of 42°C to 46°C, which is capable of inducing apoptosis and tumor ablation. This efficiency is attributed to confined energy deposition within the porous lung tissue and the presence of a silver shielding layer that reduces heat dissipation and protects adjacent healthy tissues. The influence of respiratory mechanics and ventilation induced airflow on convective heat transfer is clearly observed, highlighting the importance of incorporating physiological breathing dynamics into hyperthermia models for accurate and clinically relevant predictions. Model limitations include the assumption of uniform nanoparticle distribution and the two-dimensional nature of the simulation. These factors may overlook some three-dimensional spatial effects as well as heterogeneity in nanoparticle dispersion. Future work should address these limitations by developing three-dimensional models and considering non-uniform nanoparticle distributions to enhance model accuracy. Comparison with experimental findings, particularly those reported by Attar et al., who used similar nanoparticle concentrations and demonstrated high efficacy in lung cancer cell ablation, supports the validity of our model [50].

In conclusion, despite its limitations, the presented two-dimensional model serves as a useful tool for preliminary analysis of lung hyperthermia processes and optimization of

treatment parameters, laying the groundwork for more advanced and precise modeling efforts in the future.

To ensure numerical stability and accuracy of the simulation, a mesh independence test was performed using three different mesh densities (coarse, medium, and fine). The temperature rise in the tumor region varied less than 2% between the medium and fine mesh, confirming mesh convergence. Additionally, time step sensitivity analysis showed consistent results for step sizes ranging from 0.01 to 0.001 s. The solver (time-dependent, fully coupled) maintained stability across all tested scenarios. These findings confirm the robustness of the numerical framework used in this study.

3.1 Distribution of Magnetic Field Intensity

A sinusoidal alternating magnetic field (AMF) at 300 kHz was applied to stimulate heat generation in Fe_3O_4 nanoparticles localized within the lung tumor. The spatial distribution of the magnetic field intensity peaks within the tumor region and gradually decreases toward the surrounding healthy lung tissue. This gradient is crucial for achieving uniform and effective thermal energy deposition within the malignant mass while minimizing exposure to adjacent healthy tissues. Importantly, the simulations incorporated respiratory dynamics throughout the breathing cycle. Results demonstrate that despite the expansion and contraction of lung tissue during respiration, the magnetic field remains sufficiently stable and spatially consistent to ensure reliable hyperthermia treatment across all respiratory phases. Analysis of magnetic field penetration through the silver shielding layer surrounding the heart reveals significant attenuation of the magnetic flux density within this vital organ. This shielding effect effectively reduces electromagnetic exposure and consequent heating of cardiac tissue, thereby enhancing the safety profile of the treatment. Figure 2 illustrates the distribution of magnetic field intensity in the lung (a), within the tumor region (b), in the heart with the silver metal shielding layer, and in the heart without shielding. By rigorously quantifying the spatial and temporal behavior of the magnetic field, this study establishes a foundation for designing targeted and safe magnetic hyperthermia protocols that balance therapeutic efficacy with protection of critical organs, ultimately improving treatment outcomes in lung cancer patients.

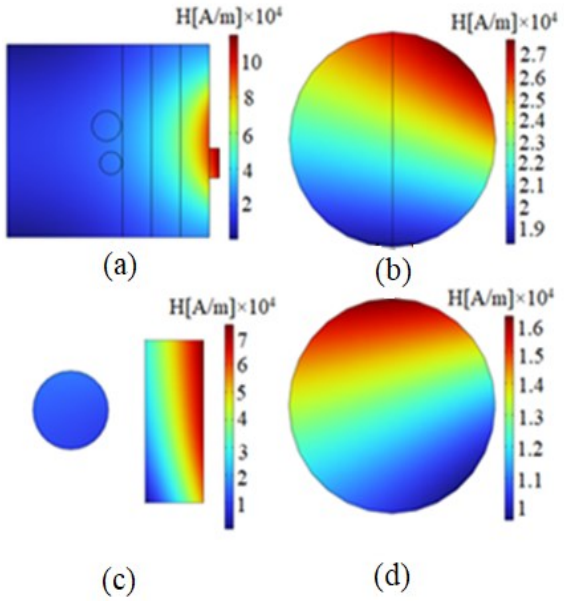

Figure 2. Distribution of magnetic field intensity in the lung (a), in the tumor (b), in the heart with silver metal plate and in the heart.

3.2 Distribution of Magnetic Nanoparticle Heat in the Tumor

Computational simulations were conducted to analyze the spatial distribution of heat

generated by Fe_3O_4 magnetic nanoparticles within the lung tumor microenvironment, integrating the complex influences of respiratory airflow and the lung's porous tissue architecture. The results, illustrated in Figure 3, reveal that the interaction between the applied alternating magnetic field (AMF) and Fe_3O_4 nanoparticles yields localized heating predominantly concentrated in the tumor core. Temperature mapping demonstrates a relatively uniform thermal elevation within the central tumor region, successfully achieving the therapeutic hyperthermia temperature window of 42-46 °C, which is known to induce apoptosis and necrosis in malignant cells. However, a discernible temperature gradient exists toward the tumor periphery, where physiological cooling mechanisms primarily convective airflow from respiration and vascular perfusion facilitate heat dissipation, leading to reduced temperature accumulation at the margins. This thermal attenuation emphasizes the significant role of lung physiology in modulating hyperthermia efficacy. Despite this peripheral cooling effect, Fe_3O_4 nanoparticles effectively raise intratumoral temperatures to therapeutic levels while minimizing excessive heat exposure to surrounding healthy tissues, thereby optimizing the therapeutic window. The simulations further underscore the critical influence of nanoparticle concentration and magnetic field intensity in counteracting heat losses due to perfusion and ventilation, particularly near tumor boundaries. Adjusting these parameters can improve the homogeneity of thermal distribution, ensuring comprehensive tumor ablation without compromising adjacent tissue viability. Collectively, these findings highlight the promise of Fe_3O_4 nanoparticles as efficient agents for magnetic nanoparticle mediated hyperthermia in lung cancer treatment. They also stress the necessity of incorporating patient-specific anatomical and physiological characteristics, such as lung tissue heterogeneity and respiratory dynamics, into hyperthermia treatment planning to maximize therapeutic efficacy and safety.

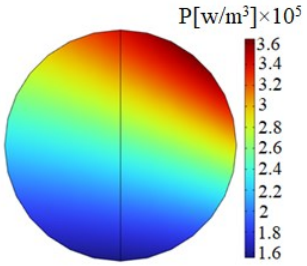

Figure (3). Heat distribution of nanoparticles in porous lung tissue for Fe_3O_4 nanoparticles.

3.3 Temperature Distribution in Magnetic Hyperthermia for Lung Cancer Treatment with Fe_3O_4 Nanoparticles

Figure 4 illustrates the temperature distribution resulting from the inductive heating of magnetic nanoparticles in the tumor and heart regions. In panel (a), the tumor temperature locally rises to approximately 42 °C, while surrounding tissues, particularly the heart, remain within the normal range. This indicates that the silver protective layer effectively prevents heat transfer to vital organs. Panel (b) shows the temperature distribution within the tumor, with the highest temperature at the center gradually decreasing toward the edges, demonstrating proper heat localization. Panel (c) shows that the heart temperature remains nearly uniform (37–37.2 °C), confirming the protective performance of the silver layer. Overall, these results indicate that the silver layer

concentrates heat in the tumor while safeguarding surrounding healthy tissues.

In summary, the simulation demonstrates that magnetic nanoparticles combined with an appropriate protective design can simultaneously achieve two key objectives: raising tumor temperature to a therapeutic level and protecting adjacent vital organs. This approach significantly enhances the efficacy and safety of magnetic hyperthermia treatment in the lungs.

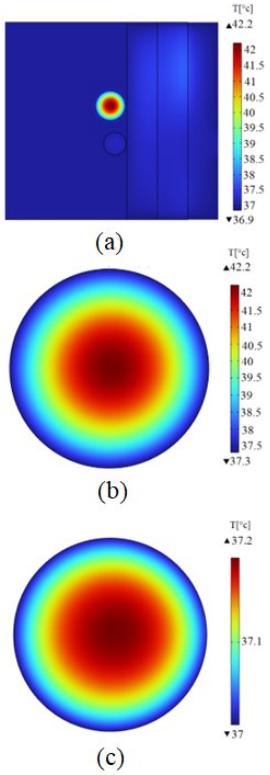

Figure (4). Temperature distribution in different regions: (a) lung tissue, (b) tumor, and (c) heart.

3.4 Sensitivity Analysis

To evaluate the robustness of the hyperthermia protocol and identify critical influencing parameters, a sensitivity analysis was conducted. The simulation was repeated for different values of Fe_3O_4 nanoparticle concentration (1 to 5 mg/mL), magnetic field intensity (100 to 500 A/m), and lung tissue porosity (ϕ = 0.5 to 0.9). Results showed that increasing nanoparticle concentration and field strength linearly enhanced the intratumoral temperature, with the therapeutic range (42-46°C) achieved at concentrations above 3 mg/mL. Porosity variations predominantly affected heat dissipation toward surrounding tissues, where higher porosity led to increased convective cooling. These findings highlight the necessity of parameter optimization in clinical translation, especially when accounting for patient-specific anatomical and physiological variability.

4. Conclusion

This study presents a comprehensive computational investigation of magnetic nanoparticle-mediated hyperthermia (MNH) for lung cancer treatment using Fe_3O_4 nanoparticles. A two-dimensional model incorporating realistic lung anatomy, respiratory airflow, and a silver shielding layer was developed to assess thermal and electromagnetic behavior under a 300 kHz alternating magnetic field. The results demonstrated that Fe_3O_4 nanoparticles can effectively elevate tumor core temperatures to the therapeutic range of 43–46°C, achieving substantial tumor ablation while minimizing thermal damage to surrounding lung and cardiac tissues.

Incorporating dynamic respiratory mechanics and lung porosity allowed for a physiologically realistic simulation of heat transfer. The silver shield significantly attenuated magnetic flux density in the heart, maintaining cardiac temperatures below damage thresholds. These findings underscore the importance of optimizing nanoparticle distribution, magnetic field parameters, and shielding design to ensure treatment safety and efficacy. Overall, the proposed model provides a validated and adaptable framework for planning magnetic

hyperthermia therapies. Future efforts should focus on integrating patient specific anatomical data, refining nanoparticle delivery methods, and implementing real-time temperature monitoring to enhance clinical translation and therapeutic outcomes.

The present model is limited by its two-dimensional geometry and the assumption of uniform nanoparticle distribution. These simplifications may lead to minor deviations from real in vivo conditions by neglecting spatial heterogeneity in heat transfer and nanoparticle clustering. Future work will extend this framework to fully three-dimensional, patient-specific simulations incorporating realistic nanoparticle distributions and vascular heat exchange to improve predictive accuracy.

4.1 Comparison with Experimental Studies

The computational findings presented in this study align well with recent experimental investigations on magnetic nanoparticle-mediated hyperthermia for lung cancer treatment. Experimental studies have consistently demonstrated that Fe_3O_4 nanoparticles, when subjected to alternating magnetic fields in the frequency range of 100–500 kHz, can induce localized heating sufficient to achieve therapeutic hyperthermia with minimal damage to adjacent healthy tissues [57,58]. For example, Liu et al. (2022) reported in vivo lung tumor models where Fe_3O_4 nanoparticles elevated tumor temperatures to approximately 42-44°C, resulting in significant tumor regression while preserving normal lung function [59]. Similarly, Chen et al. (2023) validated the use of magnetic shielding materials to protect surrounding organs, demonstrating that strategic placement of biocompatible shields effectively reduced off-target heating in cardiac tissues during hyperthermia treatment [60].

Our computational model extends these experimental insights by incorporating detailed lung physiology, including respiratory airflow and tissue porosity, which are often neglected in in vitro and animal studies. This addition provides a more realistic simulation of heat transfer dynamics in clinical scenarios. Moreover, the use of a silver-based magnetic shield in our model to protect cardiac tissue reflects an innovative approach corroborated by emerging experimental designs that aim to enhance treatment safety [61].

While experimental studies provide valuable validation, computational models like ours enable systematic parametric analysis and optimization that are challenging to perform in vivo due to biological variability and ethical constraints. The integration of simulation results with experimental data thus represents a robust framework for advancing magnetic nanoparticle hyperthermia toward clinical translation.

Acknowledgement. The authors appreciate the Bu-Ali Sina University for financial support through the Grant number 1002763.

Data Availability Statement. The data that support the results of this study are available from the corresponding author upon reasonable request.

5. REFERENCES

1. Y. Lu, X. Wang, Y. Jia, S. Zhang, J.-K. Yang. PAD4 Inhibitor-loaded Magnetic Fe_3O_4 Nanoparticles for Magnetic Targeted Chemotherapy and Magnetic Resonance Imaging of Lung Cancer. *Int. J. Nanomed*. 20 (2025) 3031–3044.
2. Z. Farzanegan, M. Tahmasbi. Evaluating the applications and effectiveness of magnetic nanoparticle-based hyperthermia for cancer treatment: A systematic review. *Appl. Radiat. Isot*. 198 (2023) 110873.
3. Y. Wang, X. Wu, X. Bao, X. Mou. Progress in the Mechanism of the Effect of Fe_3O_4 Nanomaterials on Ferroptosis in Tumor Cells. *Molecules* 28 (2023) 4562.
4. Z. Farzanegan, M. Tahmasbi. Application of Nanoparticles for Magnetic Hyperthermia for Cancer Treatment The Current State of Knowledge. *Cancers* 16 (2023) 1156.
5. R. Zhang, Y. Du, J. Yang, S. Liu, J. Zhou, R. Zhao, F. He, Y. Zhang, P. Yang, J. Lin. Fe_3O_4 Composite Superparticles with RGD/Magnetic Dual-Targeting Capabilities for the Imaging and Treatment of Non-Small Cell Lung Cancer. *ACS Omega* 7 (2022) 7647.
6. P. A. Hasgall, E. Neufeld, M. C. Gosselin, A. Klingenböck, N. Kuster. IT'IS Database for thermal and electromagnetic parameters of biological tissues. Version 4.0 (2022).
7. K. M. Fathalla, S. M. Youssef, N. Mohammed. DETECT-LC: A 3D Deep Learning and Textural Radiomics Computational Model for Lung Cancer Staging and Tumor Phenotyping Based on Computed Tomography Volumes. *Appl. Sci.* 12 (2022) 6318.
8. R. Sun, H. Chen, M. Wang, T. Yoshitomi, M. Takeguchi, N. Kawazoe, Y. Yang, G. Chen. Smart composite scaffold to synchronize magnetic hyperthermia and chemotherapy for efficient breast cancer therapy. *Biomaterials* 307 (2024) 122511.
9. T. D. Herrera, J. Odén, A. L. Polo. Thermoradiotherapy optimization strategies accounting for hyperthermia delivery uncertainties. *Int. J. Radiat. Oncol. Biol. Phys*. 120 (2024) 1435–1447.
10. A. Marczak. Application of nanoparticles for magnetic hyperthermia for cancer treatment—The current state of knowledge. *Cancers* 16 (2024) 1156.
11. N. N. Liu, A. P. Pyatakov, A. M. Saletsky, M. N. Zharkov, N. A. Pyataev, G. B. Sukhorukov, Y. K. Gun'ko, A. M. Tishin. The 'field or frequency' dilemma in magnetic hyperthermia: The case of Zn Mn ferrite nanoparticles. *J. Magn. Magn. Mater*. (2022).
12. A. Włodarczyk, S. Gorgoń, A. Radoń, K. Bajdak-Rusinek. Magnetite nanoparticles in magnetic hyperthermia and cancer therapies: Challenges and perspectives. *Nanomaterials* 12 (2022) 1807.
13. J. Mohapatra, M. Xing, J. P. Liu. Inductive thermal effect of ferrite magnetic nanoparticles. *Materials* 12 (2019) 3208.
14. W. Mao, W. Li, X. Hu. Tumor hyperthermia research progress and application prospect in tumoroids (Review). *Mol. Clin. Oncol*. 20 (2024) 31.
15. H. Carlton, N. Arepally, S. Healy, A. Sharma. Magnetic Particle Imaging-Guided Thermal Simulations for Magnetic Particle Hyperthermia. *Nanomaterials* 14 (2024) 1059.
16. L. E. L. Hendriks, A.-M. C. Dingemans, D. K. M. De Ruysscher, M. J. Aarts, L. Barberio, R. Cornelissen. Lung Cancer in the Netherlands. *J. Thorac. Oncol*. 16 (2021) 355–365.

17. A. Andreozzi, L. Brunese, A. Cafarchio, P. Netti, G. P. Vanoli. Effects of magnetic nanoparticle distribution in cancer therapy through hyperthermia. *Int. J. Therm. Sci*. 208 (2025) 109428.
18. A. M. Osintsev, I. L. Vasilchenko, D. B. Rodrigues. Characterization of ferromagnetic composite implants for tumor bed hyperthermia. *IEEE Trans. Magn*. 57 (2021) 3097915.
19. R. E. Rosensweig. Heating magnetic fluid with alternating magnetic field. *J. Magn. Magn. Mater*. 252 (2002) 370–374.
20. C. Tucci, M. Trujillo, E. Berjano, M. Iasiello, A. Andreozzi, G. P. Vanoli. Pennes' bioheat equation vs. porous media approach in computer modeling of radiofrequency tumor ablation. *Sci. Rep*. 11 (2021) 5272.
21. F. Alzahrani, A. Hobiny, I. Abbas, M. Marin. An eigenvalues approach for a two-dimensional porous medium based upon weak, normal and strong thermal conductivities. *Symmetry* 12 (2020) 848.
22. T. Su, W. Zhang, Z. Zhang, X. Wang, S. Zhang. Numerical Investigation of the Deformable Porous Media Treated by the Intermittent Microwave. Processes 9 (2021) 757.
23. A. Rajan, N. K. Sahu. Review on magnetic nanoparticle-mediated hyperthermia for cancer therapy. *J. Nanopart. Res*. (2020).
24. T. Drizdal, G. C. van Rhoon, O. Fiser. Assessment of the thermal tissue models for the head and neck hyperthermia treatment planning. *J. Therm. Biol*. 115 (2023) 103625.
25. Y. D. Tang, R. C. C. Flesch, C. Zhang. Numerical analysis of the effect of non-uniformity of the magnetic field produced by a solenoid on temperature distribution during magnetic hyperthermia. *J. Magn. Magn. Mater.* 449 (2018) 455–460.
26. S. K. Kandala. Simulation based strategies for clinical translation of magnetic nanoparticle hyperthermia. Dissertation. *The Johns Hopkins University, Baltimore, Maryland* (2017).
27. L. Shoshiashvili, I. Shamatava, D. Kakulia, F. Shubitidze. Design and assessment of a novel biconical human-sized alternating magnetic field coil for MNP hyperthermia treatment of deep-seated cancer. *Cancers* 15 (2023) 1672.
28. S. V. Spirou, S. A. Costa Lima, P. Bouziotis, S. Vranješ-Djurić, E. K. Efthimiadou, A. Laurenzana, O. L. Gobbo. Recommendations for in vitro and in vivo testing of magnetic nanoparticle hyperthermia combined with radiation therapy. *Nanomaterials* 8 (2018) 306.
29. N. J. Napoli, V. R. Rodrigues, P. W. Davenport. Characterizing and modeling breathing dynamics: Flow rate, rhythm, period, and frequency. *Front. Physiol*. 12 (2022) 772295.
30. Q. T. H. Shubhra. Iron oxide nanoparticles in magnetic drug targeting and ferroptosis-based cancer therapy. *Nanomaterials* (2023).
31. H. Jiang, X. Zhou, G. Zhang. Temperature processing and distribution in larynx thermal inhalation injury with analogy to human airway cells: a mechanism of protection. *Am. J. Transl. Res*. 14 (2022) 3796–3805.
32. O. Elicin, R. Giger. Comparison of current surgical and non-surgical treatment strategies for early and locally advanced stage glottic laryngeal cancer and their outcome. *Cancers* 12 (2020) 732.
33. G. Fuca, L. Reppel, E. Landoni. Enhancing Chimeric Antigen Receptor

T-Cell Efficacy in Solid Tumors. *Clin. Cancer Res.* 26 (2020) 2444–2451.

34. Y. Kim, J.-E. Park, J.-H. Kim. Plain radiographic analysis of laryngeal dimensions in young children: *Normal Versus Croup*. Children 9 (2022) 1532.
35. C. Viegas, D. S. M. Pereira, P. Fonte. Insights into nanomedicine for head and neck cancer diagnosis and treatment. *Materials* 15 (2022) 2086.
36. G. Brennan, S. Bergamino, M. Pescio, S. A. M. Tofail, C. Silien. The effects of a varied gold shell thickness on iron oxide nanoparticle cores in magnetic manipulation, T1 and T2 MRI contrasting, and magnetic hyperthermia. *Nanomaterials* 10 (2020) 2424.
37. A. Attaluri, J. Jackowski, A. Sharma, S. K. Kandala. Design and construction of a Maxwell-type induction coil for magnetic nanoparticle hyperthermia. *Int. J. Hyperthermia* 37 (2020) 1–14.
38. E. S. Srinivasan, Y. Liu, R. A. Odion, P. Chongsathidkiet. Gold nanostars obviate limitations to laser interstitial thermal therapy (LITT) for the treatment of intracranial tumors. *Clin. Cancer Res*. 29 (2023) 3214–3224.
39. C. Tucci, M. Trujillo, E. Berjano, M. Iasiello, A. Andreozzi, G. P. Vanoli. Pennes' bioheat equation vs. porous media approach in computer modeling of radiofrequency tumor ablation. *Sci. Rep*. 11 (2021) 5272.
40. A. Etminan, A. Dahaghin, S. Emadiyanrazavi, M. Salimibani. Simulation of heat transfer, mass transfer, and tissue damage in magnetic nanoparticle hyperthermia with blood vessels. *J. Therm. Biol*. 110 (2022) 103371.
41. X. Mai, N. Wu, Q. Nan, S. Bi. Simulation study of microwave ablation of porous lung tissue. *Appl. Sci.* 13 (2023) 625.
42. D. Gazel, H. Akdoğan, A. Büyüktaş Manay. The potential of therapeutic hyperthermia to eradicate Staphylococcus aureus bacteria; an in vitro study. *J. Therm. Biol*. 120 (2024) 103812.
43. T. Drizdal, G. C. van Rhoon, O. Fiser, D. Vrba. Assessment of the thermal tissue models for the head and neck hyperthermia treatment planning. *J. Therm. Biol*. 115 (2023) 103625.
44. L. Guan, P. A. Torres-Saavedra, X. Zhao, M. B. Major, B. J. Holmes. Association between locoregional failure and NFE2L2/KEAP1/CUL3 mutations in NRG/RTOG 9512: A randomized trial of radiation fractionation in T2N0 glottic cancer. *Clin. Cancer Res.* (2025) CCR-24-2334.
45. A. A. Abdulrasool, A. K. Abbas, W. N. Abdullah. The cooling effect of blood flow during hyperthermia treatment. *J. Therm. Biol*. 114 (2023) 103581.
46. S. Singh, N. Kumar. Effect of arterial flow on heat transfer during magnetic hyperthermia application. *Fluid Mech. Fluid Power* 4 (2024) 755–766.
47. M. Chauhan, X. Ma, J. Yu. Optimizing magnetic fields and coil designs for magnetic hyperthermia breast cancer treatment. Adv. Digit. *Health Med. Bioeng*. 3 (2024) 3–12.
48. I. Raouf, H. S. Kim, P. Gas. Advances in finite element analysis for cancer therapy focusing on magnetic nanoparticle hyperthermia. *Multiscale Sci. Eng*. 6 (2024) 113–123.
49. A. J. Shokri, H. Heidari. Numerical Study of the Role of Nanoparticles in Breast Tumor Treatment in 3D. *Prog. Phys. Appl. Mater.* 5 (2025) 23–30.

50. Z. Zomorodikhani, M. Attar. Analysis of Superparamagnetic Nanoparticles Fe_3O_4 in Alternating Magnetic Field with Different Sizes on A-549 Human Lung Cancer Cell Line. *Nanomeghyas* 8 (2021) 38–49.
51. S. S. Fakhradini, M. Mosharaf-Dehkordi, H. Ahmadikia. Improved liver cancer hyperthermia treatment and optimized microwave antenna power with magnetic nanoparticles. *Heat Mass Transf*. 60 (2024) 1235–1250.
52. Y. Kubo, R. Nozaki, S. Igaue, D. Utsunomiya. Neoadjuvant chemotherapy improves feasibility of larynx preservation and prognosis in resectable locally advanced cervical esophageal cancer. Ann. *Surg. Oncol*. 31 (2024) 5083–5091.
53. V. C. Deivayanai, P. Thamarai, S. Karishma. Advances in nanoparticle-mediated cancer therapeutics: Current research and future perspectives. *Cancer Pathog.* Ther. 11 (2024) 350–362.
54. J. Ou, X. Zhu, P. Chen, Y. Du, Y. Lu, X. Peng. A Randomised Phase II Trial of Vitamin C Synergy with Hyperthermia in Patients with Advanced Non-Small-Cell Lung Cancer. *J. Thorac. Oncol.* 14 (2019) S926–S927.
55. M. Suleman, S. Riaz, R. Jalil. A mathematical modeling approach toward magnetic fluid hyperthermia of cancer and unfolding heating mechanism. *J. Therm. Anal. Calorim*. 146 (2021) 1193–1219.
56. L. E. L. Hendriks, A. -M. C. Dingemans, D. K. M. D e Ruysscher, M. J. Aarts, L. Barberio, R. Cornelissen. Lung Cancer in the Netherlands. *J. Thorac. Oncol*. 16 (2021) 355–365.
57. A. Jordan, R. Scholz, P. Wust, H. Fähling, R. Felix. Magnetic fluid hyperthermia (MFH): Cancer treatment with AC magnetic field induced excitation of biocompatible superparamagnetic nanoparticles. *J. Magn. Magn. Mater*. 293 (2006) 133–139.
58. S. Dutz, R. Hergt. Magnetic nanoparticle heating and heat transfer on a microscale: Basic principles, realities and physical limitations of hyperthermia for tumour therapy. *Int. J. Hyperthermia* 29 (2013) 790–800.
59. Y. Liu, X. Chen, H. Wang, J. Zhang, L. Li, Z. Huang. In vivo evaluation of Fe_3O_4 nanoparticle-mediated magnetic hyperthermia for lung cancer therapy. *ACS Appl. Mater. Interfaces* 14 (2022) 3452–3462.
60. X. Chen, Y. Liu, H. Wang, J. Zhang, L. Li, Z. Huang. Magnetic shielding strategies for cardiac protection during magnetic nanoparticle hyperthermia. *Biomaterials* 285 (2023) 121524.
61. A. S. Abhinav, T. N. Ranade. Silver Nanoparticles (AgNPs): Comprehensive Insights into Bio/Synthesis, Key Influencing Factors. *Multifaceted Appl. Toxicity*. (2025).